Atomic Layer Deposition of Lithium Phosphorus Oxynitride

Mikko Nisula,[†] Yohei Shindo,[‡] Hideyuki Koga,[‡] and Maarit Karppinen*[,†]

[†]Department of Chemistry, Aalto University, FI-00076 Aalto, Finland
[‡]Higashifuji Technical Center, Toyota Motor Co., 1200 Mishuku, Susono, Japan

ABSTRACT: An atomic layer deposition (ALD) process is successfully developed for fabricating high-quality lithium phosphorus oxynitride (LiPON) thin films for a potential use as a conformal solid-state electrolyte coating in 3D Li-ion microbattery technology. In our ALD process the challenge of simultaneously incorporating phosphorus and nitrogen in the films is overcome by using a novel nitrogen-containing phosphorus precursor, diethyl phosphoramidate, together with lithium hexamethyldisilazide as the lithium precursor. A temperature window is found around 270−310 °C, where homogeneous films are realized and the film growth is controlled in a digital manner by the number of ALD cycles at a rate of ~0.7 Å/cycle. The process allows for a high N-to-P ratio in the films, which is beneficial for achieving the required high ionic conductivity. For a film deposited at 330 °C with a composition of $Li_{0.95}PO_{3.00}N_{0.60}$ according to RBS/NRA analysis, an ionic conductivity value as high as 6.6×10^{-7} S cm^{-1} is measured at 25 °C.
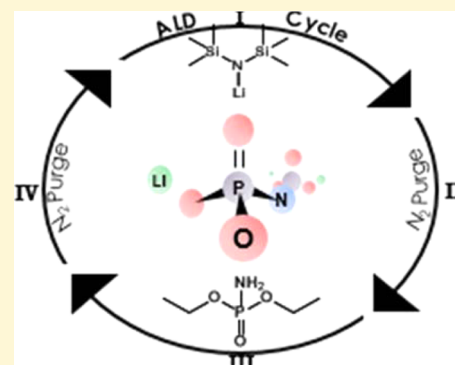
1. INTRODUCTION

The ever increasing power consumption of portable electronic devices has left the current lithium ion battery (LIB) technology lagging behind. The two-dimensional (2D) structure of the liquid-electrolyte-based cells places limitations on the energy density per surface area. By switching over to all-solid-state LIBs, the energy density can be increased by three-dimensional (3D) structures with vastly increased surface areas as the technology allows for more flexible design concepts. Moreover, the all-solid-state LIBs are inherently safer due to the chemically stable solid electrolyte.[1−3]

A crucial part of a solid-state Li-ion battery is the electrolyte, for which the 3D microbatteries place stringent requirements. The ionic conductivity of the electrolyte needs to be high to minimize the internal resistance, while the electronic conductivity of it should be negligible to prevent the self-discharge of the cell. Furthermore, the electrolyte needs to be electrochemically stable across a wide potential range, and to be chemically inert against both the anode and the cathode materials.

Lithium phosphorus oxynitride (LiPON) possesses a number of highly beneficial material properties, being thus one of the frontier electrolyte material options for solid-state LIBs: its ionic conductivity is relatively high, up to 10^{-6} S cm^{-1}, while the parasitic electronic conductivity is very low,[4] the electrochemical stability window is rather high, and the material is stable even against a metallic Li anode. The current fabrication methods of LiPON coatings include methods such as sputtering,[5] pulsed laser deposition,[6] and MOCVD.[7] Unfortunately, none of these thin-film techniques is particularly suitable for fabricating the pinhole-free and conformal electrolyte coatings on high-aspect-ratio nanostructures being imperative for the 3D microbattery technologies.

Atomic layer deposition (ALD) is a uniquely superior gas-phase thin-film technique for depositing highly conformal coatings with atomic-level precision on complex nanometer-scale architectures.[8] This is achieved by the sequential introduction of the different precursors to the reactor chamber. Due to the self-limiting nature of the underlying gas-surface reactions, the film growth is terminated during each precursor pulse once the surface is saturated.

So far thermal ALD processes have been developed for some potential solid-state electrolyte materials such as lithium lanthanum titanate,[9] lithium phosphate,[10,11] lithium tantalate,[12] Li_xAl_yO,[13] and $Li_xAl_ySi_zO$,[14] but not—to our best knowledge—for LiPON. Here, it should be mentioned that, after the initial submission of the present paper, Kozen et al.[15] reported a four-precursor plasma-ALD process for LiPON films. Attempts to combine the existing Li_3PO_4[10] and Li_3N[16] ALD processes based on trimethyl phosphate and ammonia precursors, respectively, have proven unfruitful. We suspect that this is due to the difficulty in forming the P−N bonds when $(CH_3)_3PO_4$ and NH_3 are employed as precursors. It has been reported that, in the gas phase, NH_3 almost exclusively undergoes a nucleophilic substitution at the carbon of the methyl ester group instead of cleaving the P−O bonds to form the required P−N bonds.[17] Thus, we decided to test a completely different approach and selected a route where a nitrogen-containing phosphorus precursor is utilized. In this way, the aforementioned issue could be circumvented. Here we report the successful deposition of LiPON thin films by ALD, utilizing a novel precursor, diethyl phosphoramidate. The new ALD process,

moreover, allows high N-to-P ratios in the films, which has been shown to be beneficial to the ionic conductivity of LiPON.[18] Our LiPON thin films exhibit an order of magnitude higher ionic conductivity values compared to those reported for other ALD-grown lithium solid electrolyte materials.

2. EXPERIMENTAL SECTION

The LiPON thin films were deposited using an F-120 flow-type hot-wall ALD reactor (ASM Microchemistry Ltd.) from lithium hexamethyldisilazide $LiN(SiMe_3)_2$ (LiHMDS) and diethyl phosphoramidate $H_2NP(O)(OC_2H_5)_2$ (DEPA) precursors. The other common lithium precursor, lithium $tert$-butoxide (LiO^{t}Bu), was also briefly evaluated and film growth was observed with growth rates comparable to those for LiHMDS. However, LiHMDS was chosen over LiO^{t}Bu due to its better stability in ambient atmosphere. The precursors were kept inside the reactor, LiHMDS at 60 °C and DEPA at 87 °C. Nitrogen (99.999%) was used both as a carrier and purging gas with a flow rate of 300 sccm. It was produced from air by a nitrogen generator (Schmidlin UHPN 3000). The films were deposited on 3.5 × 3.5 cm^2 Si(100) and borosilicate substrates. The substrates were cleaned with ethanol in an ultrasonic bath before use. The pressure in the reactor was ~5 mbar, and the depositions were carried out at different temperatures from 230 to 350 °C. In order to determine the sublimation temperature of DEPA, it was investigated by a combined thermogravimetric/differential scanning calorimetry (TG/DSC) analysis in a Netzsch STA 449 C Jupiter thermobalance under ca. 1.5 mbar pressure. The heating rate was 10 °C/min, and the sample mass was ca. 20 mg.

The thickness of the films was determined with X-ray reflection (XRR), and their amorphous nature was confirmed by grazing incidence X-ray diffraction (GIXRD); both measurements were carried out using a PANalytical X'Pert Pro diffractometer with a Cu K$_\alpha$ X-ray source. The scanning electron microscopy (SEM) images were obtained using a Zeiss Sigma VP FE-SEM. The elemental depth profile of the films was investigated with Rutherford backscattering spectrometry (RBS) and nuclear reaction analysis (NRA) using a National Electrostatic Corporation Pelletron 3SDH. The RBS measurements were carried out by using a 2.3 MeV He ion beam with a scattering angle of 110°, while the Li content was determined by $^7Li(p,\alpha)^4He$ NRA using a 1.5 MeV proton beam with a scattering angle of 146°. X-ray photoemission spectroscopy (XPS) and Fourier transform infrared spectroscopy (FTIR) were utilized to analyze the chemical state of the samples deposited on Si. The XPS measurements were carried out with a PHI Quantera SMX instrument with monochromatic Al Kα radiation (1486.6 eV). The diameter of the irradiated area was 200 μm. The binding energy was calibrated based on the C 1s peak set to 284.6 eV. The FTIR measurements were carried out in transmission mode on samples consisting of 1200 deposition cycles using a Nicolet Magna 750 spectrometer in the 4000−400 cm^{-1} region at a 2 cm^{-1} resolution.

Ionic conductivity of the films was evaluated with electrochemical impedance spectroscopy (EIS) with an Autolab PGSTAT302N potentiostat/galvanostat in a frequency range of 200 kHz to 10 Hz. A "cross plane" type of measurement setup was utilized where the thin film sample, totaling 1200 deposition cycles, was sandwiched between two Au electrodes as described in ref 5. The electrodes were prepared via thermal evaporation (Leybold-Heraeus UNIVEX300), and the geometric area of the electrodes was 0.2 × 0.2 cm^2. The EIS measurements were conducted under Ar atmosphere. The electronic conductivity of the films was determined by chronoamperometry with an applied potential of 50 mV using the same measurement setup.

3. RESULTS AND DISCUSSION

We first investigated the thermal behavior of DEPA in order to reveal its suitability as a precursor for our ALD process. In Figure 1 the TG/DSC curves measured for DEPA are shown. The DSC plot reveals two exothermic peaks at ca. 60 and 115 °C, assigned to represent the melting and subsequent
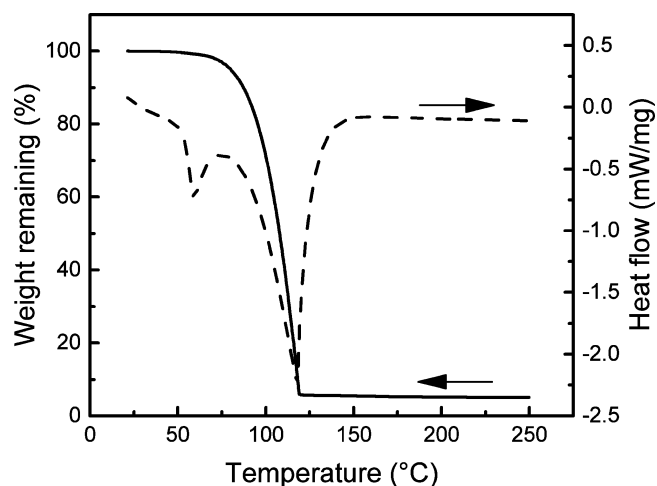

Figure 1. TG (solid line) and DSC (dashed line) curves for DEPA recorded under ca. 1.5 mbar pressure with a heating rate of 10 °C/min.

evaporation of DEPA. The onset temperature for evaporation as determined from the TG curve is ca. 95 °C. No sign of decomposition of DEPA is seen, and the residue is as low as 5%.

The growth-per-cycle (GPC) values achieved using pulse and purge lengths of 2 s for each precursor in our ALD process for the LiPON films are plotted as a function of deposition temperature in Figure 2. The growth rate is relatively stable
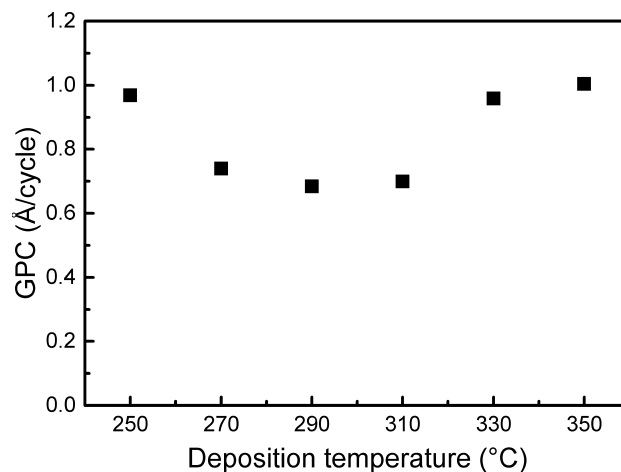

Figure 2. Growth per cycle (GPC) for the LiHMDS-DEPA process as a function of deposition temperature. The number of ALD cycles was fixed at 1200. The pulse and purge lengths for both precursors were 2 s.

between 270 and 310 °C at around 0.7 Å/cycle. For the lower temperature depositions at 250 °C, a somewhat higher growth rate of 0.96 Å/cycle was observed, and visually the films appeared to be slightly unevenly colored. At 230 °C a film was yet obtained, but it was visually very uneven, and the thickness could not be determined with XRR. From Figure 2, the growth rate increases also when the deposition temperature is increased from 310 °C. However, unlike the films deposited at temperatures below 270 °C, those deposited at 330 and 350 °C were evenly colored from visual observation. GIXRD measurements revealed that the thin films were amorphous across the whole deposition temperature range.

In order to demonstrate the surface saturation limited growth characteristic of ALD, the growth rate was further studied at 290 °C by varying the pulse lengths of both LiHMDS and DEPA. As can be seen from Figure 3, a pulse length of 2 s is
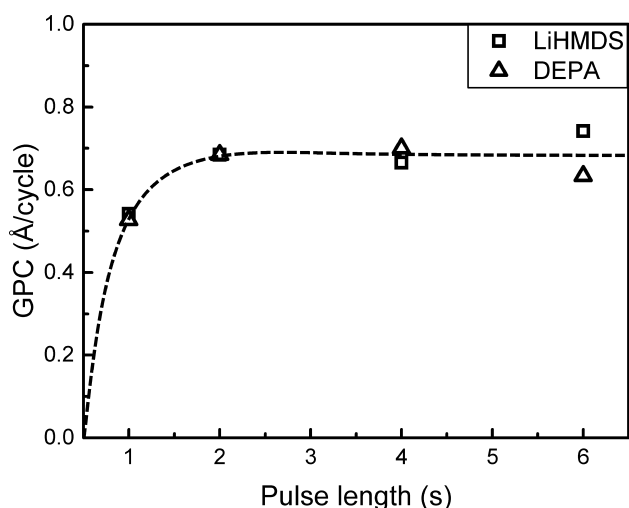

Figure 3. Growth per cycle of LiPON thin films as a function of LiHMDS (squares) and DEPA (triangles) pulse lengths. The pulse length for the other precursor and the purge lengths were fixed to 2 s. The deposition temperature was 290 °C, and the number of ALD cycles was fixed to 600. The dashed line only serves as a guide to the eye.

indeed enough for both precursors to achieve the full surface saturation. Moreover, as shown in Figure 4 the thickness of the
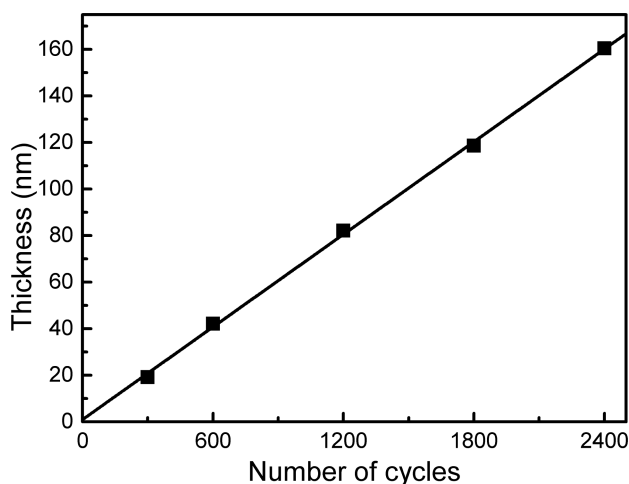

Figure 4. Thickness of the LiPON films as a function of the number of deposition cycles. The deposition temperature was 290 °C. The solid line was obtained via regression analysis of the data with the origin not included, $R^2 = 0.999$.

LiPON films deposited at 290 °C is linearly dependent on the number of deposition cycles. It is to be noted that at temperatures above 310 °C full saturation for LiHMDS was not achieved, indicating that at these temperatures the precursor presumably starts to suffer from thermal decomposition.

Given the requirement for the solid state electrolyte to uniformly coat complicated 3D structures, the conformality of the LiPON ALD process was tested on a micron scale trench

pattern ~40 μm deep and ~5 μm wide. The pulse and purge lengths were extended to 4 s for both precursors to ensure full coverage. A total of 1200 cycles were applied at a deposition temperature of 290 °C. The SEM images in Figure 5 reveal that the resultant thin film is very uniform in thickness at the top and the bottom parts of the trench, and even the nanoscale roughness of the substrate is perfectly replicated. Moreover, the thickness is measured to be ~80 nm, which is in excellent agreement with the thickness results on planar substrates. The FTIR spectra for films deposited at 290 and 330 °C are presented in Figure 6; the sample thicknesses were 82 and 115 nm, respectively. According to Senevirathne et al.[19] the main feature at around 1000 cm^{-1} consists of several overlapping absorption peaks arising from P−O (938 cm^{-1}, 1016 cm^{-1}) and P−N vibrations (850 cm^{-1}, 1055 cm^{-1}, 1115 cm^{-1}). The peak at ~500 cm^{-1} is apparently due to the Li−O−P bond.[20] A small feature at ~2950 cm^{-1} arises from stretching vibrations of C−H bonds in saturated aliaphatic species which might indicate the presence of a carbohydrate residue from either precursor. The peak at ~2300 cm^{-1} is due to background CO_2 in the FTIR apparatus. The lack of antisymmetric C−O stretching at 1400−1500 cm^{-1} indicates that Li_2CO_3 is not formed during the deposition or after brief exposure to ambient atmosphere.[21] Interestingly, no telltale signs of the amine group of DEPA, namely N−H stretching at 3300−3400 cm^{-1} and NH$_2$ bending at ~1600 cm^{-1},[22] can be discerned. Given the very low intensity of the C−H stretching, these results would indicate that both the -NH$_2$ and the -OEt groups participate in the deposition reaction.

Elemental compositions determined by RBS-NRA and XPS for films deposited at 290 and 330 °C are presented in Table 1. There is a marked discrepancy between the measured values, with the XPS results showing much higher lithium and carbon contents. It is known that LiPON degrades in humid air,[23] and while great care was taken to limit the exposure of the samples to ambient atmosphere, it was not possible to eliminate it entirely. Thus, it is likely that Li_2CO_3 is formed on the film surface during the sample storing before the XPS and RBS-NRA measurements. The elemental depth profiles as determined by RBS-NRA (Figure 7) reveal that the amount of carbon is higher at the surface of the films, further suggesting the presence of a thin Li_2CO_3 surface layer.

While in the film deposited at 330 °C the carbon is mainly concentrated to the very top surface layer, in the film deposited at 290 °C the amount of carbon remains high much deeper into the film. The concentrations of Li, P, N, and O remain nearly constant relative to each other, indicating otherwise a rather homogeneous thin film. The thermal decomposition of LiHMDS should be seen as Si impurity in the samples. The XPS data show Si contents of 0.7 and 1.1 atom % for the films deposited at 290 and 330 °C, respectively, whereas in the RBS data no Si is detected except at the thin film−substrate interface. Thus, the decomposition of LiHMDS appears to be rather limited even at the higher deposition temperature.

The average elemental concentrations as determined by RBS-NRA correspond to compositions of $Li_{0.90}PO_{2.75}N_{0.55}$ and $Li_{0.95}PO_3N_{0.60}$ for the films deposited at 290 and 330 °C, respectively. As such, the Li/P ratio is relatively low compared to the previously reported values of 2.6−4.0 for LiPON films deposited by sputtering,[18,24−26] but it would be consistent with an ALD growth model where LiHMDS preferentially reacts with the ethyl ester groups of DEPA, in which case each Li atom would be shared between two adjacent phosphoramidate
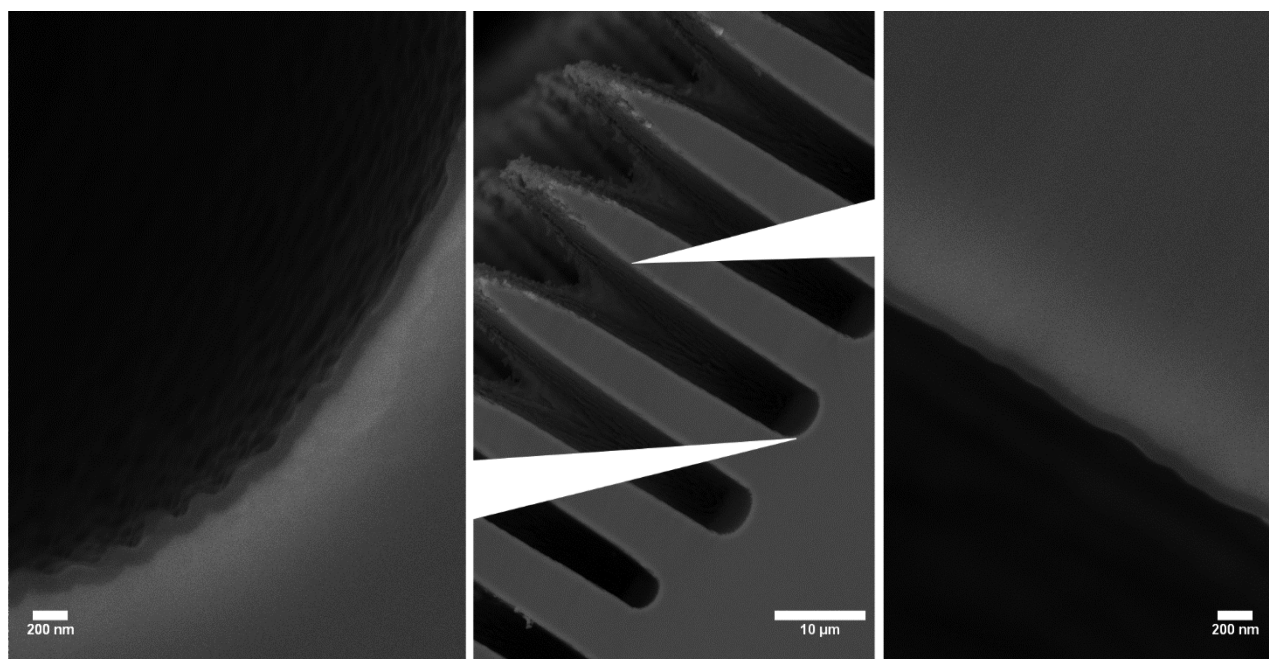
Figure 5. Cross section SEM images of LiPON deposited of 3D-microstructured silicon.
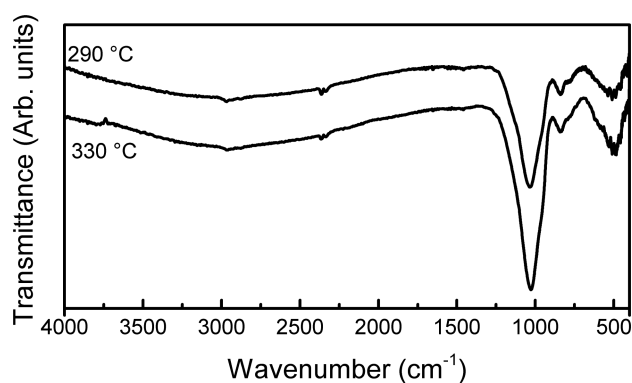

Figure 6. FTIR spectra for LiPON films deposited at 290 and 330 °C.

Table 1. Elemental Composition of the LiPON Films Deposited at 290 and 330 °C as Determined by RBS-NRA and XPS

Deposition temp	Atomic conc (%)				
	Li	P	N	O	C
RBS-NRA					
290 °C	15.0	16.6	9.1	45.8	13.3
330 °C	15.4	16.2	9.7	48.7	9.9
XPS					
290 °C	21.7	3.4	2.3	35.0	35.9
330 °C	21.0	2.8	2.1	33.4	39.0

Figure 7. Elemental depth profiles for LiPON films deposited at 290 °C, and 330 °C, from RBS-NRA analysis.

groups. The O-to-P ratio of ca. 3 and absence of signs of aliaphatic carbon further indicate the carbon−oxygen bond acting as one reactive site. The lower than nominal ratio of the N-to-P ratio could suggest that here the reaction would proceed either through the N−H bond or by removal of the whole −NH$_2$ group. One hypothetical scheme could be the cross-linking of two PO$_3$N$_x$ groups:
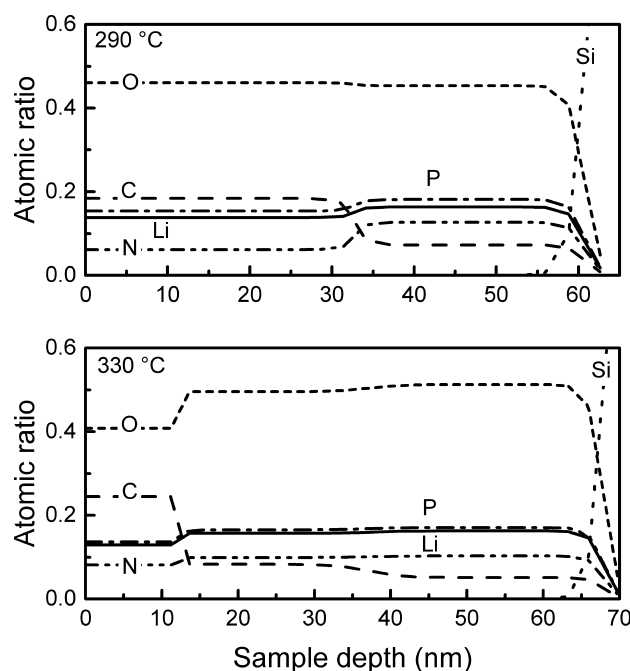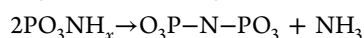
$$2PO_3NH_x \rightarrow O_3P-N-PO_3 + NH_3$$

Given that ALD precursors should not be self-reacting and saturation limited growth was indeed observed, the aforementioned reaction must also involve the presence of lithium.

The XPS core spectra of N 1s, O 1s, P 2p, and C 1s are presented in Figure 8. The N 1s spectra are deconvoluted into two pseudo-Voigt components attributed to doubly and triply coordinated nitrogen (inset of Figure 8).[18,24,27,28] It is apparent that the triply coordinated nitrogen at a binding energy of 398.9 eV (±1 eV) is the dominant component in both samples, while the amount of doubly coordinated nitrogen at 397.4 eV (±1 eV) appears to decrease with increasing deposition temperature. In the C 1s spectra two peaks are present. The one at
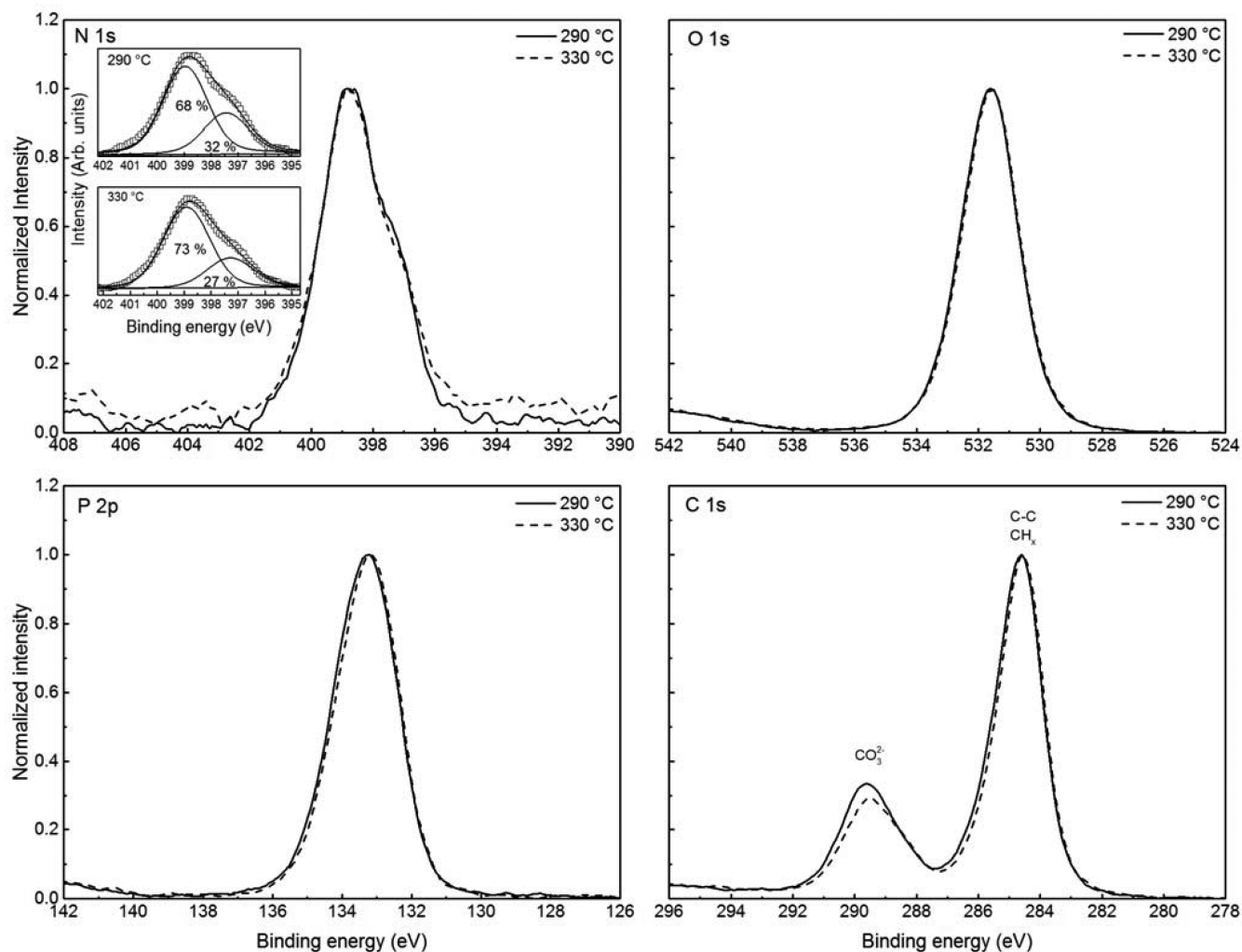
Figure 8. XPS spectra at N 1s, O 1s, P 2p, and C 1s for LiPON films deposited at 290 (solid line) and 330 °C (broken line). The inset of the top left panel represents the deconvolution result of the N 1s spectra.
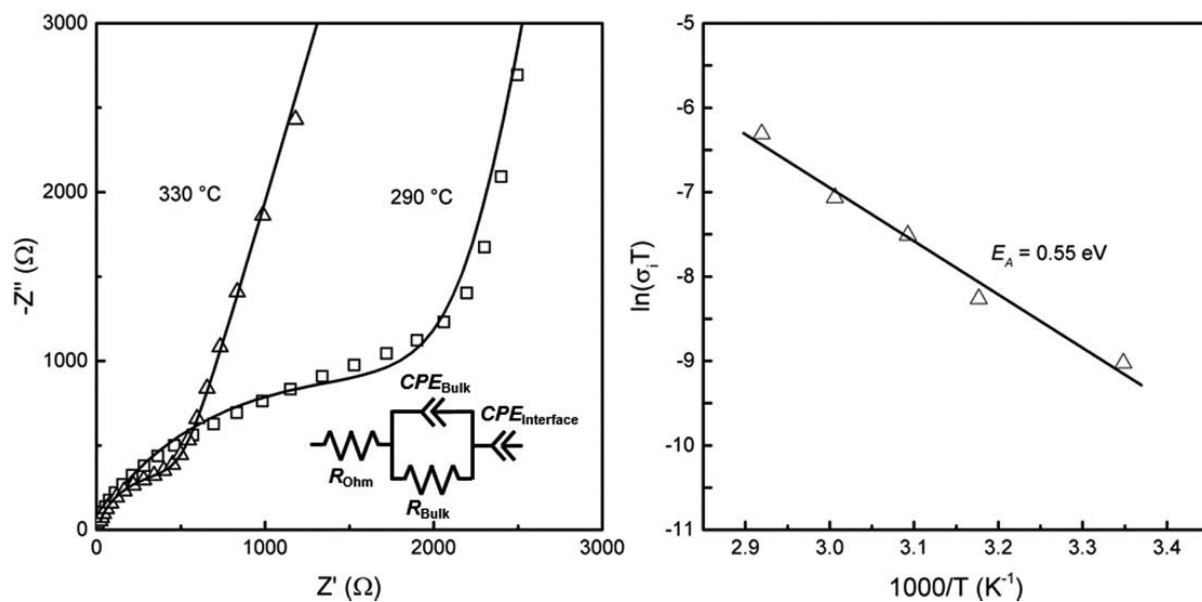

Figure 9. On the left, impedance plots for LiPON films deposited at 290 (squares) and 330 °C (triangles). The measurement temperature was 25 °C. The solid lines represent the fitted values obtained using the equivalent circuit depicted in the inset. On the right, the Arrhenius plot of the ionic conductivity for a LiPON film deposited at 330 °C.

284.6 eV corresponds to hydrocarbons originating from the precursors and as atmospheric impurity, while the second one at 289.6 eV indicates the presence of CO_3^{2-} groups, further pointing out to the presence of Li_2CO_3 on the film surface. As such, while deconvolution of the O 1s peak would have provided additional information on the film structure,[18] it was not attempted, as the contribution from the carbonate impurity could not be distinguished from the main phase. In the P 2p spectra, no significant difference between the two samples is observed: the peaks being centered at 133.2 eV. The peaks are located at a slightly lower binding energy than that of Li_3PO_4 (133.8 eV),[29] which is consistent with previous results where a shift to a lower binding energy was associated with the increase in the nitrogen content.[18]

Room-temperature ionic conductivity was determined for the films deposited at 290 and 330 °C using electrochemical impedance spectroscopy. The acquired Nyqvist plots presented on the left side in Figure 9 consist of a semicircle in the high-frequency region followed by an inclined tail in the low-frequency region. The high-frequency semicircle is attributed to the bulk resistance of the film, while the inclined tail arises from the polarization of the electrode−electrolyte interface.[12] Such features are typical for an ionic conductor when the measurement is conducted using an ion-blocking electrode material such as Au (as was used in this work). The impedance spectra were fitted using an equivalent circuit depicted in the inset of Figure 9. In the equivalent circuit, R_{Ohm} represents the contact resistance and the constant phase element $CPE_{interface}$ models the polarization of the electrode−electrolyte interface. The bulk response is modeled by parallel R_{Bulk} and CPE_{Bulk}.

The ionic conductivity, σ_i, can be determined by the equation, $\sigma_i = d/(R_{bulk}A)$, where d is the thickness of the sample (82 and 115 nm for the 290 and 330 °C sample, respectively) and A is the geometric area of the electrodes. At 298 K, ionic conductivity values of 9.3×10^{-8} S cm^{-1} and 6.6×10^{-7} S cm^{-1} are obtained for the films deposited at 290 and 330 °C, respectively. For the former film the high frequency semicircle is highly flattened and could actually be composed of two overlapping semicircles. Such a phenomenon can be attributed to an additional resistive layer such as Li_2CO_3, which is consistent with the XPS data. As such, the results agree with those very recently reported by Kozen et al.[15] for LiPON thin films deposited by plasma-ALD (3.36×10^{-7} S cm^{-1} for comparable nitrogen content), indicating that the nitrogen content is not the sole determining factor for the magnitude of the ionic conductivity.

The electronic conductivity values as determined from the steady state current of the chronoamperometry measurements are 3×10^{-12} and 3×10^{-11} S cm^{-1} for the films deposited at 290 and 330 °C, respectively. The values are in line with the value of $8.6 \pm 0.4 \times 10^{-12}$ S cm^{-1} reported for sputtered LiPON thin films.[30] As the electronic conductivity is 4 orders of magnitude lower than the conductivity values obtained from the EIS measurements, it can be concluded that the EIS data represents the actual ionic conductivity of our LiPON thin films.

The activation energy for the ionic conductivity for the film deposited at 330 °C was obtained using the Arrhenius equation, $\sigma_i T = A \exp[-E_a/(kT)]$, where A is a pre-exponential factor, E_a is the activation energy of ionic conduction, k is Boltzmann's constant, and T is absolute temperature. As shown on the right side of Figure 9, the activation energy was determined to be

0.55 eV, which is in good agreement with previously reported values for sputtered LiPON films.[5]

4. CONCLUSIONS

We presented a new promising ALD process to deposit high-quality LiPON thin films from LiHMDS and DEPA precursors in a well-controlled manner. The key insight in the process development was to employ a nitrogen-containing phosphorus precursor to directly transfer the required P−N bond into the resultant LiPON film. An essentially constant growth rate of 0.7 Å/cycle was achieved in the deposition temperature range of 270−310 °C. The films were found to be amorphous, and the presence of nitrogen was confirmed with RBS-NRA measurements. The XPS data furthermore implied that the amount of triply coordinated nitrogen increased with increasing deposition temperature. The ionic conductivity of our LiPON thin films deposited at 330 °C was measured to be as high as 6.6×10^{-7} S cm^{-1} at room temperature, with the activation energy determined to be 0.55 eV. The straightforward waterless binary process should be advantageous when considering the up-scalability, and thus we believe that our LiPON ALD process has true potential to play an important role in the emerging all-solid-state Li-ion microbattery technology.

■ AUTHOR INFORMATION

Corresponding Author
*E-mail: maarit.karppinen@aalto.fi.

Notes
The authors declare no competing financial interest.

■ ACKNOWLEDGMENTS

■ REFERENCES

(1) Long, J. W.; Dunn, B.; Rolison, D. R.; White, H. S. Three-Dimensional Battery Architectures. *Chem. Rev.* **2004**, *104*, 4463−4492.

(2) Oudenhoven, J. F. M.; Baggetto, L.; Notten, P. H. L. All-Solid-State Lithium-Ion Microbatteries: A Review of Various Three-Dimensional Concepts. *Adv. Energy Mater.* **2011**, *1*, 10−33.

(3) Roberts, M.; Johns, P.; Owen, J.; Brandell, D.; Edstrom, K.; El Enany, G.; Guery, C.; Golodnitsky, D.; Lacey, M.; Lecoeur, C.; Mazor, H.; Peled, E.; Perre, E.; Shaijumon, M. M.; Simon, P.; Taberna, P.-L. 3D Lithium Ion Batteries—from Fundamentals to Fabrication. *J. Mater. Chem.* **2011**, *21*, 9876.

(4) Le Van-Jodin, L.; Ducroquet, F.; Sabary, F.; Chevalier, I. Dielectric Properties, Conductivity and Li+ Ion Motion in LiPON Thin Films. *Solid State Ionics* **2013**, *253*, 151−156.

(5) Yu, X.; Bates, J. B.; Jellison, G. E.; Hart, F. X. A Stable Thin-Film Lithium Electrolyte: Lithium Phosphorus Oxynitride. *J. Electrochem. Soc.* **1997**, *144*, 524.

(6) Zhao, S.; Fu, Z.; Qin, Q. A Solid-State Electrolyte Lithium Phosphorus Oxynitride Film Prepared by Pulsed Laser Deposition. *Thin Solid Films* **2002**, *415*, 108−113.

(7) Kim, H. T.; Mun, T.; Park, C.; Jin, S. W.; Park, H. Y. Characteristics of Lithium Phosphorous Oxynitride Thin Films Deposited by Metal-Organic Chemical Vapor Deposition Technique. *J. Power Sources* **2013**, *244*, 641−645.

(8) Meng, X.; Yang, X.-Q.; Sun, X. Emerging Applications of Atomic Layer Deposition for Lithium-Ion Battery Studies. *Adv. Mater.* **2012**, *24*, 3589−3615.

(9) Aaltonen, T.; Alnes, M.; Nilsen, O.; Costelle, L.; Fjellvåg, H. Lanthanum Titanate and Lithium Lanthanum Titanate Thin Films Grown by Atomic Layer Deposition. *J. Mater. Chem.* **2010**, *20*, 2877−2881.

(10) Hämäläinen, J.; Holopainen, J.; Munnik, F.; Hatanpää, T.; Heikkilä, M.; Ritala, M.; Leskelä, M. Lithium Phosphate Thin Films Grown by Atomic Layer Deposition. *J. Electrochem. Soc.* **2012**, *159*, A259−A263.

(11) Wang, B.; Liu, J.; Sun, Q.; Li, R.; Sham, T.-K.; Sun, X. Atomic Layer Deposition of Lithium Phosphates as Solid-State Electrolytes for All-Solid-State Microbatteries. *Nanotechnology* **2014**, *25*, 504007.

(12) Liu, J.; Banis, M. N.; Li, X.; Lushington, A.; Cai, M.; Li, R.; Sham, T. K.; Sun, X. Atomic Layer Deposition of Lithium Tantalate Solid-State Electrolytes. *J. Phys. Chem. C* **2013**, *117*, 20260−20267.

(13) Aaltonen, T.; Nilsen, O.; Magrasó, A.; Fjellvåg, H. Atomic Layer Deposition of Li2O−Al2O3 Thin Films. *Chem. Mater.* **2011**, *23*, 4669−4675.

(14) Perng, Y.-C.; Cho, J.; Sun, S. Y.; Membreno, D.; Cirigliano, N.; Dunn, B.; Chang, J. P. Synthesis of Ion Conducting Li X Al Y Si Z O Thin Films by Atomic Layer Deposition. *J. Mater. Chem. A* **2014**, *2*, 9566−9573.

(15) Kozen, A. C.; Pearse, A. J.; Lin, C.-F.; Noked, M.; Rubloff, G. W. Atomic Layer Deposition of the Solid Electrolyte LiPON. *Chem. Mater.* **2015**, *27*, 5324−5331.

(16) Østreng, E.; Vajeeston, P.; Nilsen, O.; Fjellvåg, H. Atomic Layer Deposition of Lithium Nitride and Carbonate Using Lithium Silylamide. *RSC Adv.* **2012**, *2*, 6315.

(17) Hodges, R.; Sullivan, S. A.; Beauchamp, J. L. Nucleophilic Reactions of Anions with Trimethyl Phosphate in the Gas Phase by Ion Cyclotron Resonance Spectroscopy. *J. Am. Chem. Soc.* **1980**, *102*, 935−938.

(18) Fleutot, B.; Pecquenard, B.; Martinez, H.; Letellier, M.; Levasseur, a. Investigation of the Local Structure of LiPON Thin Films to Better Understand the Role of Nitrogen on Their Performance. *Solid State Ionics* **2011**, *186*, 29−36.

(19) Senevirathne, K.; Day, C. S.; Gross, M. D.; Lachgar, A.; Holzwarth, N. a W. A New Crystalline LiPON Electrolyte: Synthesis, Properties, and Electronic Structure. *Solid State Ionics* **2013**, *233*, 95−101.

(20) Belous, a. G.; V'yunov, O. I.; Kovalenko, L. L.; Bohnke, O.; Bohnke, C. Synthesis of Thin-Film Electrodes Based on LiPON and LiPON-LLTO-LiPON. *Russ. J. Electrochem.* **2014**, *50*, 523−530.

(21) Brooker, M. H.; Bates, J. B. Raman and Infrared Spectral Studies of Anhydrous Li2CO3 and Na2CO3. *J. Chem. Phys.* **1971**, *54*, 4788−4796.

(22) Chiang, C.-H.; Ishida, H.; Koenig, J. L. The Structure of Γ-Aminopropyltriethoxysilane on Glass Surfaces. *J. Colloid Interface Sci.* **1980**, *74*, 396−404.

(23) Nimisha, C. S.; Rao, G. M.; Munichandraiah, N.; Natarajan, G.; Cameron, D. C. Chemical and Microstructural Modifications in LiPON Thin Films Exposed to Atmospheric Humidity. *Solid State Ionics* **2011**, *185*, 47−51.

(24) Roh, N. S.; Lee, S. D.; Kwon, H. S. Effects of Deposition Condition on the Ionic Conductivity and Structure of Amorphous Lithium Phosphorus Oxynitrate Thin Film. *Scr. Mater.* **1999**, *42*, 43−49.

(25) Choi, C. H.; Cho, W. I.; Cho, B. W.; Kim, H. S.; Yoon, Y. S.; Tak, Y. S. Radio-Frequency Magnetron Sputtering Power Effect on the Ionic Conductivities of Lipon Films. *Electrochem. Solid-State Lett.* **2002**, *5*, A14.

(26) Park, H. Y.; Nam, S. C.; Lim, Y. C.; Choi, K. G.; Lee, K. C.; Park, G. B.; Lee, S.-R.; Kim, H. P.; Cho, S. B. Effects of Sputtering Pressure on the Characteristics of Lithium Ion Conductive Lithium Phosphorous Oxynitride Thin Film. *J. Electroceram.* **2006**, *17*, 1023−1030.

(27) Wang, B.; Kwak, B. S.; Sales, B. C.; Bates, J. B. Ionic Conductivities and Structure of Lithium Phosphorus Oxynitride Glasses. *J. Non-Cryst. Solids* **1995**, *183*, 297−306.

(28) Mascaraque, N.; Fierro, J. L. G.; Durán, A.; Muñoz, F. An Interpretation for the Increase of Ionic Conductivity by Nitrogen Incorporation in LiPON Oxynitride Glasses. *Solid State Ionics* **2013**, *233*, 73−79.

(29) Morgan, W. E.; Van Wazer, J. R.; Stec, W. J. Inner-Orbital Photoelectron Spectroscopy of the Alkali Metal Halides, Perchlorates, Phosphates, and Pyrophosphates. *J. Am. Chem. Soc.* **1973**, *95*, 751−755.

(30) Nowak, S.; Berkemeier, F.; Schmitz, G. Ultra-Thin LiPON Films − Fundamental Properties and Application in Solid State Thin Film Model Batteries. *J. Power Sources* **2015**, *275*, 144−150.